Published in final edited form as:
Cell. 2012 October 26; 151(3): 630–644. doi:10.1016/j.cell.2012.10.011.

MICU1 is an Essential Gatekeeper for MCU-Mediated Mitochondrial Ca^{2+} Uptake That Regulates Cell Survival

Karthik Mallilankaraman[1,6,#], **Patrick Doonan**[1,6,#], **César Cárdenas**[2,3,#], **Harish C. Chandramoorthy**[1,6,#], **Marioly Muller**[2], **Russell Miller**[4], **Nicholas E. Hoffman**[1,6], **Rajesh Gandhirajan**[1,6], **Jordi Molgó**[5], **Morris J. Birnbaum**[4], **Brad Rothberg**[1], **Don-On Daniel Mak**[2], **J. Kevin Foskett**[2,7,*], and **Muniswamy Madesh**[1,6,*]

[1]Department of Biochemistry, Temple University, Philadelphia, Pennsylvania 19140, USA

[2]Department of Physiology, University of Pennsylvania, Philadelphia, Pennsylvania 19104, USA

[3]Anatomy and Developmental Biology Program, Institute of Biomedical Sciences, University of Chile, Santiago, 4 Chile

[4]Institute for Diabetes, Obesity and Metabolism, University of Pennsylvania, Philadelphia, PA 19104, USA

[5]CNRS, Institute de Neurobiologie Alfred Fessard, FRC2118, Laboratoire de Neurobiologie Cellulaire et Moléculaire, UPR 3294, CNRS, 91198 Gif-sur-Yvette cedex, France

[6]Center for Translational Medicine, Temple University, Philadelphia, Pennsylvania, 19140, USA

[7]Department of Cell and Developmental Biology, University of Pennsylvania, Philadelphia, Pennsylvania 19104, USA

SUMMARY

Mitochondrial Ca^{2+} (Ca^{2+}_m) uptake is mediated by an inner membrane Ca^{2+} channel called the uniporter. Ca^{2+} uptake is driven by the considerable voltage present across the inner membrane ($\Delta\Psi_m$) generated by proton pumping by the respiratory chain. Mitochondrial matrix Ca^{2+} concentration is maintained 5–6 orders of magnitude lower than its equilibrium level, but the molecular mechanisms for how this is achieved are not clear. Here we demonstrate that the mitochondrial protein MICU1 is required to preserve normal $[Ca^{2+}]_m$ under basal conditions. In its absence, mitochondria become constitutively loaded with Ca^{2+}, triggering excessive reactive oxygen species generation and sensitivity to apoptotic stress. MICU1 interacts with the uniporter pore-forming subunit MCU and sets a Ca^{2+} threshold for Ca^{2+}_m uptake without affecting the kinetic properties of MCU-mediated Ca^{2+} uptake. Thus, MICU1 is a gatekeeper of MCU-mediated Ca^{2+}_m uptake that is essential to prevent $[Ca^{2+}]_m$ overload and associated stress.

*To whom correspondence should be addressed: Muniswamy Madesh, Center for Translational Medicine, Department of Biochemistry, 3500 N. Broad Street, 950 MERB, Temple University, Philadelphia, PA 19140, Phone: (215) 707 5465, Fax: (215) 707 9890, madeshm@temple.edu. J. Kevin Foskett, Department of Physiology, 726 Clinical Research Bldg., 415 Curie Blvd., University of Pennsylvania, Philadelphia, PA 19104-6085, Phone: (215) 898–1354, foskett@mail.med.upenn.edu.
#These authors contributed equally to this manuscript.

INTRODUCTION

Mitochondrial Ca^{2+} homeostasis plays important roles in cellular physiology. Ca^{2+} flux across the inner mitochondrial membrane (IMM) regulates cell bioenergetics, cytoplasmic Ca^{2+} ($[Ca^{2+}]_i$) signals and activation of cell death pathways (Balaban, 2009; Denton and McCormack, 1980; Duchen et al., 2008; Gunter and Gunter, 1994; Hajnoczky et al., 1995; Hansford, 1994; Herrington et al., 1996; Lemasters et al., 2009; McCormack et al., 1990; Orrenius et al., 2003; Szalai et al., 1999). Mitochondrial Ca^{2+} ($Ca^{2+}{}_m$) uptake has been studied for over five decades, with crucial insights into the underlying mechanisms enabled by development of the chemi-osmotic hypothesis and appreciation of the considerable voltage across the IMM ($\Delta\Psi_m$) generated by proton pumping in the respiratory chain (Carafoli, 1987; Drago et al.; Nicholls, 2005; O'Rourke, 2007; Rottenberg and Scarpa, 1974). Ca^{2+} uptake is an electrogenic process driven by $\Delta\Psi_m$ and mediated by a Ca^{2+} selective ion channel (MiCa (Kirichok et al., 2004) called the uniporter (Bernardi, 1999; Igbavboa and Pfeiffer, 1988; O'Rourke, 2007; Santo-Domingo and Demaurex, 2010). Properties of the uniporter have been derived primarily from studies of isolated mitochondria, where it was generally found to have a low apparent Ca^{2+} affinity (10–70 μM) with variable cooperativity (Bragadin et al., 1979; Gunter et al., 1994). Agonist-induced $[Ca^{2+}]_i$ signals can be rapidly transduced to the mitochondrial matrix despite this apparent low affinity because mitochondria can exist in close apposition to sites of Ca^{2+} release where local $[Ca^{2+}]_i$ can be higher than in the bulk cytoplasm (Carafoli and Lehninger, 1971; Collins et al., 2001; Filippin et al., 2003; Nicholls, 2008; Palmer et al., 2006; Rizzuto et al., 2004; Rizzuto et al., 1998). Nevertheless, higher affinity mitochondrial Ca^{2+} uptake has been observed in many studies (Santo-Domingo and Demaurex, 2010; Spat et al., 2008). Furthermore, patch clamp electrophysiology suggests that the uniporter pore has high Ca^{2+} affinity (dissociation constant < 2 nM) that enables it to have high Ca^{2+} selectivity (Kirichok et al., 2004). In addition, the open probability of the uniporter channel is voltage dependent, reaching nearly unity at normal $\Delta\Psi_m$ (~−180 mV) (Kirichok et al., 2004). Thus, whereas rapid and substantial $Ca^{2+}{}_m$ uptake can take place in regions of high $[Ca^{2+}]_i$ micro-domains, the high open probability and Ca^{2+} affinity of the uniporter pore suggest that the large thermodynamic driving force for Ca^{2+} uptake would result in $Ca^{2+}{}_m$ overload in the absence of regulatory mechanisms to limit the activity of the channel. However, the identity of such mechanisms remains elusive.

Until recently, the molecular identity of the uniporter was unknown. MICU1 was identified as a protein that localized to the IMM and suggested to be required for uniporter-mediated Ca^{2+} uptake (Perocchi et al., 2010). Subsequently, MCU was identified as the likely ion-conducting pore of the uniporter (Baughman et al., 2011; De Stefani et al., 2011). MICU1 and MCU biochemically interact, and their expression patterns are tightly coupled across tissues and species (Baughman et al., 2011). Nevertheless, the functional relationship between these two uniporter components is unknown.

Here, we report that loss of MICU1 leads to constitutive $Ca^{2+}{}_m$ accumulation through MCU. MICU1 is not required for MCU-mediated $Ca^{2+}{}_m$ uptake. Instead, MICU1 is a gatekeeper for MCU-mediated Ca^{2+} uptake, establishing a threshold (the set-point) that prevents Ca^{2+} uptake in low $[Ca^{2+}]_i$ (< 3 μM), but does not confer low apparent Ca^{2+} affinity or cooperativity of MCU-mediated Ca^{2+} uptake at higher $[Ca^{2+}]_i$. MICU1 regulation of MCU requires each of its Ca^{2+} binding EF hands, suggesting that they provide the high-affinity $[Ca^{2+}]$ sensing mechanism that enables MICU1 to exert its regulation. MICU1 senses matrix $[Ca^{2+}]$, since it inhibits MCU-mediated Ca^{2+} uptake only when $[Ca^{2+}]_m$ is low. These findings reveal a previously unknown role of MICU1 as a gatekeeper to limit MCU-mediated Ca^{2+} influx to prevent $Ca^{2+}{}_m$ overload and its associated stress under resting conditions.

RESULTS

Knockdown of MICU1 Causes Basal Ca^{2+}_m Accumulation

HeLa cells were transfected with MICU1 siRNA (Table S1) to silence its expression or a non-targeting scrambled siRNA as control (Figure S1A). Strikingly, $[Ca^{2+}]_m$ was constitutively elevated under resting conditions in MICU1 knock down (KD) cells (Figures S1B and 1C). It was previously reported that MICU1 expression was required for uniporter-mediated Ca^{2+} uptake (Perocchi et al., 2010). Nevertheless, MICU1 KD did not affect the ability of mitochondria to accumulate Ca^{2+} in response to an agonist-induced $[Ca^{2+}]_i$ rise (Figures S1D, 1E and 1G). Nor did it affect the magnitude of a histamine-induced $[Ca^{2+}]_i$ rise (Figure S1F) or $\Delta\Psi_m$ (Figure S1H).

MCU was identified as the pore forming subunit of the mitochondrial uniporter (Baughman et al., 2011; De Stefani et al., 2011). To confirm that MICU1 and MCU KD are not functionally equivalent, we compared effects of knocking down expression of either protein in independent assays. We previously demonstrated that inhibition of basal inositol trisphosphate receptor ($InsP_3R$)-mediated Ca^{2+} release resulted in insufficient Ca^{2+} transfer from ER to mitochondria to support optimal bioenergetics. As a consequence, cellular [AMP]:[ATP] ratio is elevated and autophagy is activated as a pro-survival mechanism (Cardenas et al., 2010). If MCU and MICU1 are each required for Ca^{2+}_m uptake, we speculated that KD of either protein would elevate [AMP]:[ATP] and induce autophagy. Nevertheless, whereas [AMP]:[ATP] was increased in MCU KD cells, it was unchanged in MICU1 KD cells (Figure S1I). Elevated autophagy was observed (Cardenas et al., 2010) in MCU KD, but it was unchanged in MICU1 KD cells (Figure S1J, S1K). Whereas the effects of MCU KD are as expected if MCU plays an essential role in Ca^{2+}_m uptake, those of MICU1 are not. These results strengthen the conclusion that MICU1 is not essential for Ca^{2+}_m uptake, and support the notion that it plays a distinct role.

We generated stable clones using lentiviral shRNAs targeting different regions of the MICU1 gene (Table S2 and Figure S1L). Two, shHe#B4 and shHe#B6, had 80.7% and 82.6% mRNA KD, respectively (Figure S1L). We used clone shHe#B6 for subsequent experiments. As in cells treated with MICU1 siRNA, $[Ca^{2+}]_m$ was constitutively elevated in stable MICU1 KD cells (Figure 1A and 1B), with elevated basal $[Ca^{2+}]_m$ correlated with the degree of KD (Figure 1B, and see Figure S1L). Also as in siRNA-treated cells, histamine-induced Ca^{2+}_m uptake (Figure 1C and 1E) and rise of $[Ca^{2+}]_i$ (Figure 1D) were unaltered in MICU1 KD cells. Nor was $\Delta\Psi_m$ (Figure 1F) or [AMP]:[ATP] (Figure S1M) affected, and autophagy was not activated (Figure S1N). Lack of autophagy induction in MICU1 KD cells was not due to intrinsic defects in autophagy since Xestospongin B (XeB), a specific $InsP_3R$ inhibitor, induced autophagy similarly in control (shHe#B8) and KD cells (Figure S1N). We extended these studies to human endothelial cells (EC) with MICU1 stably knocked down. Similar to HeLa cells, $[Ca^{2+}]_m$ was constitutively elevated (Figures 1G and 1H), whereas histamine-induced Ca^{2+}_m uptake (Figure 1I and 1K) and rise of $[Ca^{2+}]_i$ (Figure 1J) were unaffected and $\Delta\Psi_m$ was normal (Figure 1L).

Defective Ca^{2+}_m uptake can result in enhanced agonist-induced $[Ca^{2+}]_i$ responses due to diminished cytoplasmic buffering (Hoth et al., 2000; Simpson and Russell, 1998). In agreement, $[Ca^{2+}]_i$ was elevated for a prolonged period in response to histamine in MCU KD cells, whereas a transient response was observed in MICU1 KD cells (Figure S1O). The Ca^{2+} dependent transcription factor NFAT was strongly activated in MCU KD cells, consistent with the prolonged $[Ca^{2+}]_i$ signal, whereas only weak activation was observed in MICU1 KD cells (Figure S1P). Further, nuclear NFATC3-GFP positive cells showed increased nuclear translocation in MCU-silenced cells compared with MICU1 KD cells (Figures S1Q and S1R).

Together these results suggest that MICU1 is not required for uniporter-dependent Ca^{2+} uptake, nor does it function similarly to MCU. Instead, they suggest that MICU1 may play a role in constitutively suppressing $Ca^{2+}{}_m$ uptake under resting conditions.

Constitutive $Ca^{2+}{}_m$ Accumulation in MICU1 KD Cells Occurs Through MCU-Mediated Ca^{2+} Uptake

We confirmed (Perocchi et al., 2010) that MICU1 biochemically interacts with MCU (Figure S2A). MICU1 KD did not alter MCU expression (Figure S2B). We therefore considered that MICU1 may function to inhibit MCU-mediated Ca^{2+} uptake, and that the observed elevated basal $[Ca^{2+}]_m$ in MICU1 ablated cells occurs through uncontrolled MCU-dependent Ca^{2+} uptake. To test this, we silenced MCU expression by >85% (Figure S2C) in control neg shRNA and MICU1 KD HeLa and ECs (Figure S2D). Histamine-induced $Ca^{2+}{}_m$ uptake was effectively abrogated, demonstrating functional efficacy of MCU KD (Figure 2C, 2E). Importantly, silencing MCU abolished elevated basal $[Ca^{2+}]_m$ in MICU1 KD cells (Figure 2A–E). This indicates that Ca_m^{2+} accumulation induced by loss of MICU1 is mediated by MCU-dependent Ca^{2+} uptake. To further verify this, we assessed $Ca^{2+}{}_m$ uptake in digitonin-permeabilized stable HEK293 cells (Figure S2E) bathed in intracellular-like medium (ICM) containing thapsigargin (Tg) to prevent ER Ca^{2+} uptake and FuraFF to monitor $[Ca^{2+}]$ in the medium. Following exposure of control cells to Tg, Ca^{2+} leak from the ER caused ICM $[Ca^{2+}]$ to increase progressively over ~5 min to ~ 1.8 μM (Figure 2F). Subsequent exposure to the MCU inhibitor Ru360 had little effect (Figure 2F), indicating that mitochondria had not taken up Ca^{2+}. In contrast, ICM $[Ca^{2+}]$ did not increase during ER Ca^{2+} leakage from MICU1 KD cells (Figure 2F). Subsequent exposure to Ru360 caused a rapid rise of ICM $[Ca^{2+}]$ to levels observed in control cells (Figure 2F and 2G). These results indicate that Ru360-sensitive MCU-dependent Ca^{2+} uptake buffered Ca^{2+} released from the ER in the MICU1 KD cells. Further, the observation that Ca^{2+} efflux was active in MICU1 KD cells, evident upon addition of Ru360, indicates that MICU1 KD does not alter $Ca^{2+}{}_m$ efflux (Figure 2F, also see Figure S5). Importantly, this buffering occurred in MICU1 KD cells at $[Ca^{2+}]$ under which MCU-dependent Ca^{2+} uptake is normally not active. Accordingly, these results suggest that MICU1 normally acts as a brake to prevent MCU-dependent $Ca^{2+}{}_m$ uptake at low $[Ca^{2+}]_i$.

To test this further, we examined phosphorylation of the mitochondrial protein pyruvate dehydrogenase (PDH). PDH phosphorylation by pyruvate kinase suppresses its activity whereas dephosphorylation by Ca^{2+}-dependent pyruvate dehydrogenase phosphatase (PDP) enhances it (Cardenas et al., 2010). If MICU1 normally acts to prevent MCU-mediated Ca^{2+} uptake under basal conditions, we speculated that PDH would be constitutively hypo-phosphorylated in MICU1 KD cells by enhanced Ca^{2+}-activated PDP activity. In agreement, PDH was hypo-phosphorylated in MICU1KD cells (Figure S2F). As a control, XeB, which blocks ER Ca^{2+} release (Cardenas et al., 2010), increased PDH phosphorylation in the MICU1 KD cells to levels comparable to those in the control cells (Figure S2G).

MICU1 Inhibits MCU-Mediated $Ca^{2+}{}_m$ Influx in Low $[Ca^{2+}]$

Our results suggest that MICU1 may regulate the apparent Ca^{2+} affinity or threshold of MCU-dependent Ca^{2+} uptake. To examine this in more detail, we used the permeabilized cell protocol and simultaneously monitored the rate of $Ca^{2+}{}_m$ uptake and $\Delta\Psi_m$ in response to boluses of Ca^{2+} added to ICM. Cells (~6 million) were permeabilized in ICM containing Tg. After 450s, a single bolus of Ca^{2+} was added, and the Fura FF (Figure 3A) and JC-1 (Figure 3B) signals were monitored for 300s before an uncoupler (CCCP) was added to depolarize the IMM and release accumulated Ca^{2+} (Figure 3A and 3F). Ca^{2+} uptake in these conditions, monitored as a decrease in ICM $[Ca^{2+}]$, is completely dependent on MCU (Figure 3G). In response to a 0.5 μM Ca^{2+} bolus, ICM $[Ca^{2+}]$ rapidly rose to a stable plateau

in control cells, indicating lack of Ca^{2+}_m uptake at this $[Ca^{2+}]$, as expected. In contrast, ICM $[Ca^{2+}]$ decreased to nearly the pre-pulse level in MICU1 KD cells (Figure 3A). Subsequent CCCP addition released significantly more Ca^{2+} from MICU1 KD mitochondria, indicating that the decrease in ICM $[Ca^{2+}]$ following the initial pulse was due to Ca^{2+}_m uptake (Figure 3F, and see inset). Similarly, in response to a 1 μM Ca^{2+} pulse, Ca^{2+} uptake in control cells was absent, whereas uptake in MICU1 KD cells was substantial (Figure 3A). The difference in Ca^{2+}_m uptake between control and MICU1 KD cells was not due to a greater driving force for Ca^{2+} uptake in MICU1 KD cells, since $\Delta\Psi_m$ both before and during the Ca^{2+} pulses were similar in control and KD cells (Figure 3B) and MICU1 KD mitochondria have higher basal $[Ca^{2+}]_m$ (Figure 1B, 1H, 2B and 2D). In addition, it cannot be accounted for by different expression levels of MCU (Figure S2B). In response to a 2 μM Ca^{2+} pulse, control mitochondria buffered the $[Ca^{2+}]$, but to a level (the set-point (Nicholls, 2005)) that was significantly higher than that achieved by MICU1 KD mitochondria (Figure 3A). At higher concentrations (5–50 μM), both control and MICU1 KD cells exhibited robust Ca^{2+}_m uptake (Figure 3A) with similar transient $\Delta\Psi_m$ depolarizations at 20 and 50 μM pulses (Figure 3B). Reconstitution of MICU1 (Figure S2E and 2G) in MICU1 KD HeLa cells prevented elevated basal $[Ca^{2+}]_m$ and reverted Ca^{2+}_m uptake (Figure 2A–E). Similarly, rescue of MICU1 in permeabilized HEK293 cells prevented elevated basal $[Ca^{2+}]_m$ and reverted Ca^{2+}_m uptake in response to low $[Ca^{2+}]$ bolus additions (1–5 μM) to control levels (Figure S3A–D).

The ICM $[Ca^{2+}]$ decay kinetics were all well fitted assuming a single exponential process. The fits were used to calculate the change in ICM $[Ca^{2+}]$ due to Ca^{2+}_m uptake following the pulse, as well as the rate of Ca^{2+}_m uptake. Mitochondria in MICU1 KD cells took up more Ca^{2+} than control cells in the low $[Ca^{2+}]$ regime, from 0.5 to ~5 μM (Figure 3C inset). In contrast, MICU1 KD was without consequence at higher $[Ca^{2+}]$ (Figure 3C). Surprisingly, Hill equation fits of the uptake rates yielded similar kinetic parameters in control and MICU1 KD cells (Figure 3D). The K_d, or apparent Ca^{2+}af finity of Ca^{2+}_m uptake, was ~11 μM in control and MICU1 KD cells, with Hill coefficients of 3.2 and 3.4, respectively (Figure 3E). These results suggest that MICU1 plays an important role in limiting Ca^{2+}_m uptake in the low $[Ca^{2+}]$ regime, without affecting the overall kinetic behavior of MCU-mediated Ca^{2+} uptake. The total amount of Ca^{2+} buffered by control and MICU1 KD mitochondria in response to the Ca^{2+} pulses was evaluated by measuring the amount of Ca^{2+} released by CCCP (Figure 3F). Mitochondria with MICU1 knocked down took up more Ca^{2+} than control mitochondria in the low $[Ca^{2+}]$ regime, up to 5 μM Ca^{2+}. Notably, however, the amount taken up vs. $[Ca^{2+}]$ curve for the two groups was parallel over the entire range of $[Ca^{2+}]$ (Figure 3F), with the offset between them accounted for by Ca^{2+} accumulated by MICU1 KD mitochondria before the pulses (the offset in Figure 3A). These results demonstrate that MICU1 KD does not change Ca^{2+}_m buffering capacity. Taken together, these data suggest that MICU1 acts as a "gatekeeper" that sets a $[Ca^{2+}]$ threshold to prevent Ca^{2+}_m uptake in low $[Ca^{2+}]_i$, but it does not play a role in conferring the well-established cooperativity of Ca^{2+}_m uptake.

MICU1 is a Gatekeeper of MCU-mediated Ca^{2+}_m Influx

Our results suggest that MICU1 regulates MCU-dependent Ca^{2+}_m uptake in low $[Ca^{2+}]$. First, mitochondria in MICU1 KD cells have constitutively elevated $[Ca^{2+}]_m$ (Figures 1A–C, 1G–1I and 2A–2E). This suggests that in absence of MICU1, MCU-mediated Ca^{2+} uptake is active at $[Ca^{2+}]_i$ that exists in resting cells. Second, mitochondria in permeabilized MICU1 KD cells take up Ca^{2+} from boluses added to the ICM at concentrations (up to ~3 μM) where control mitochondria do not (Figures 3A and 3C). Third, in response to slow addition of Ca^{2+} to the medium (in permeabilized cells caused by ER Ca^{2+} leak), ICM Ca^{2+} is unbuffered and consequently rises in control cells, but is buffered by Ca^{2+}_m uptake in

MICU1 KD cells (Figure 3A and 4A). During the 450 s following Tg-induced ER leak, ICM $[Ca^{2+}]$ rose by nearly 1 μM to 1.8 ± 0.06 μM in control cells, but by only ~160 nM to 0.9 ± 0.02 μM in MICU1 KD cells (Figure 4B and 4C), similar to the set-point value reported previously (Nicholls, 1978). MICU1 KD mitochondria also reduced ICM $[Ca^{2+}]$ to lower levels than controls following acute Ca^{2+} pulses. Following Ca^{2+} pulses in the 0.5 – 5 μM regime, MICU1 KD mitochondria reduced ICM $[Ca^{2+}]$ during the subsequent 300 sec to 1.3 μM, whereas control mitochondria reduced it to 2.7 μM (Figure 4D and 4E), similar to the ~3 μM threshold determined (Figure 3C and Figure S3E). In response to higher $[Ca^{2+}]$ pulses (Figure 4F), mitochondria in both cells rapidly buffered Ca^{2+}, but MICU1 KD mitochondria reduced ICM $[Ca^{2+}]$ to ~1.9 μM, whereas control mitochondria buffered it less effectively to a higher level, again to ~3 μM (Figure 4G and 4H).

Elevated $[Ca^{2+}]_m$ stimulates oxidative phosphorylation (OX-PHOS) by activating mitochondrial enzymes (Denton and McCormack, 1980; Hajnoczky et al., 1995; Robb-Gaspers et al., 1998). $InsP_3$-linked agonists trigger large increases in $[Ca^{2+}]_m$ because close appositions between mitochondria and ER enables released Ca^{2+} to reach levels sufficient for rapid and substantial permeation through MCU. If MICU1 acts as a gatekeeper to set the $[Ca^{2+}]_i$ threshold for $Ca^{2+}{}_m$ uptake, we speculated that its absence would enable agonist-induced $[Ca^{2+}]_i$ signals to more efficiently raise $[Ca^{2+}]_m$ within the total mitochondrial population by enabling those that lack close appositions to ER to take up released Ca^{2+}. We hypothesized that such recruitment would enable weak agonist stimulation to more efficaciously enhance OX-PHOS. In control cells, low (10 μM) histamine was without effect on O_2 consumption rate (OCR) (Figure S4A–B) whereas it was enhanced over 3-fold in response to 100 μM histamine (Figure S4C–D). In contrast, OCR was enhanced by over 2-fold in response to 10 μM histamine in MICU1 KD cells, nearly to the level achieved by 100 μM histamine (Figure S4A–D). These results are consistent with the hypothesis that MICU1 regulates the threshold $[Ca^{2+}]_i$ for MCU-dependent $Ca^{2+}{}_m$ uptake.

EF Hand Domains of MICU1 Regulate the Ca^{2+} Threshold for MCU-Mediated Ca^{2+} Uptake

Our results indicate that MICU1 regulates the threshold for MCU–mediated Ca^{2+} uptake in the low Ca^{2+} regime extending down to resting $[Ca^{2+}]_i$, suggesting that it senses $[Ca^{2+}]$ with high affinity. MICU1 contains two highly-conserved Ca^{2+}-binding EF hands. We speculated that high-affinity Ca^{2+} binding by the EF hands enables MICU1 to sense low $[Ca^{2+}]$ to inhibit MCU. To test this, we stably re-expressed in MICU1 KD cells shRNA-insensitive MICU1 with either EF1 or EF2 hands disabled by introduction of two point mutations of critical acidic residues that disable Ca^{2+} binding (Figure 5A). As shown previously in Figures S3A–D, re-expression of shRNA-insensitive MICU1 rescued the MICU1 KD cells, preventing MCU-dependent $Ca^{2+}{}_m$ uptake in permeabilized cells in response to elevated ICM $[Ca^{2+}]$ induced by release of ER stores, or in response to an acute 1 μM Ca^{2+} pulse. In contrast, re-expression of MICU1 with either EF1 or EF2 mutated (Figure 5A) failed to rescue MICU1 KD cells (Figure 5B–E). Interestingly, Hill equation fits of the uptake rates of cells stably expressing MICU1 with either EF hand mutated yielded kinetic parameters similar to those of control and MICU1 KD cells (Figure 5F and 5G). Thus, MICU1 regulation of the $[Ca^{2+}]$ threshold for MCU-mediated Ca^{2+} uptake is mediated by high affinity Ca^{2+} binding by its two EF hands.

MICU1 EF hands are located in the mitochondrial matrix (Perocchi et al., 2010). Accordingly, MICU1 should respond to $[Ca^{2+}]_m$. To test whether MICU1 senses $[Ca^{2+}]_m$ specifically, permeabilized cells were exposed to a single 10 μM Ca^{2+} pulse. Both control and MICU1 KD cells rapidly take up Ca^{2+} and reduce ICM $[Ca^{2+}]$ to a new steady state level similar to that present before the pulse (Figure 3A and Figure S5). Before the pulse, MCU-mediated Ca^{2+} uptake at this ICM $[Ca^{2+}]$ was minimal in control cells, as evidenced by lack of significant Ca^{2+} extrusion observed upon block of Ca^{2+} uptake by Ru360, in

contrast to the behavior of MICU1 KD cells (Figure 2F). However, after the pulse both control and MICU1 KD cells behaved similarly, exhibiting robust MCU-mediated Ca^{2+} uptake, as evidenced by the high rate of Ca^{2+} extrusion mediated by the Na^{+}/Ca^{2+} exchanger upon Ru360 addition (Figure S5). Thus, the elevation of $[Ca^{2+}]_m$ after the 10 μM pulse relieved MICU1 inhibition of MCU-mediated Ca^{2+} uptake, indicating that MICU1 senses resting matrix $[Ca^{2+}]$ specifically.

MICU1 Deficiency Elevates Basal Mitochondrial ROS Generation and Sensitizes Cells to Apoptotic Cell Death

Mitochondrial OX-PHOS and NADPH oxidases are the major ROS sources in most cells (Hamanaka and Chandel, 2010; Lambeth, 2004). $Ca^{2+}{}_m$ overload is associated with excessive mitochondrial ROS (mROS) generation (Jacobson and Duchen, 2002). Basal mROS levels were elevated by several-fold in MICU1 KD cells (Figure 6A – C). Elevated mROS in MICU1 KD cells was unaltered by the NADPH oxidase inhibitor DP1, whereas the mitochondrial complex III blocker Antimycin A elevated mROS in both cell types (Figure 6C). This indicates that NADPH oxidases are not responsible for mROS elevation in MICU1 KD cells. Importantly, either reconstitution of MICU1 or siRNA silencing of MCU in MICU1 KD cells abrogated mROS elevation (Figure 6D). Similar results were obtained in ECs (Figure 6E and 6F). Thus, failure of MICU1 to inhibit MCU-mediated Ca^{2+} uptake under low $[Ca^{2+}]_i$ conditions results in $[Ca^{2+}]_m$-dependent mROS overproduction. Whereas constitutively elevated $[Ca^{2+}]_m$ in MICU1 KD cells was expected to enhance basal bioenergetics, this was not observed (Figure S4). We asked whether elevated basal mROS inhibited mitochondrial metabolism. MICU1 KD cells were transduced for 36 hr with mitochondrial (manganese superoxide dismutase; AdMnSOD) and cytosolic (glutathione peroxidase 1; AdGPX1) antioxidants. Both markedly decreased [AMP]:[ATP] (Figure S6A) and enhanced basal OCR (Figure S6B), suggesting that chronic $[Ca^{2+}]_m$ elevation, by generating excessive mROS, inhibited Ca^{2+}-activated OX-PHOS.

Physiological mROS is implicated in many processes including gene expression, cell growth, proliferation and differentiation, whereas excessive mROS promotes cell death (Balaban et al., 2005; Hamanaka and Chandel, 2010). Chronic mROS elevation in MICU1 KD HeLa cells did not alter proliferation (Figure 7A). However, MICU1 KD ECs had defective migration in a wound-healing assay (Figure 7B). Strikingly, ceramide-induced HeLa cell death (Figure S7A and S7B) was enhanced by nearly 100% in MICU1 KD cells (Figure 7C) and lipopolysaccharide + cycloheximide (LPS/CHX) induced EC death was enhanced by MICU1 KD (Figure 7D). Importantly, cell death was prevented in MICU1 rescue cells (Figure 7C and D). Over-expression of antioxidant mitochondrial MnSOD and cytoplasmic GPX1 also strongly protected MICU1 KD cells (Figure 7C and 7D). Thus, MICU1 inhibition of MCU-dependent Ca^{2+} uptake under basal conditions is necessary to suppress $Ca^{2+}{}_m$ accumulation, excessive mROS production and sensitivity to apoptotic stress.

DISCUSSION

The most significant finding of our studies is that MICU1 plays an essential role in limiting $Ca^{2+}{}_m$ uptake when $[Ca^{2+}]_i$ is low, within the range found in cells at rest or during weak agonist stimulation. In absence of this regulation, mitochondria become constitutively loaded with Ca^{2+} under resting conditions, and they more effectively take up Ca^{2+} in low $[Ca^{2+}]_i$. Whereas the latter effect enables cells to respond more sensitively to weak agonist stimulation, the former effect has detrimental effects, including enhanced mROS generation and susceptibility to cell stresses. MICU1 provides an essential protective mechanism by limiting MCU-mediated Ca^{2+} uptake in the face of a tremendous thermodynamic driving

force. This essential role likely accounts for the tightly correlated expression and physical interaction of MICU1 and MCU.

MICU1 is a Gatekeeper of MCU-mediated Mitochondrial Ca^{2+} Influx

Our results suggest that MICU1 inhibits MCU-dependent Ca^{2+} uptake in low $[Ca^{2+}]$. Mitochondria in MICU1 KD cells have constitutively elevated $[Ca^{2+}]_m$, suggesting that MICU1 limits MCU-mediated Ca^{2+} uptake at $[Ca^{2+}]_i$ that exists in resting cells, ~ 50–100 nM. Even at such low $[Ca^{2+}]_i$, the thermodynamic driving force for Ca^{2+} uptake across the IMM is prodigious (Azzone et al., 1977; Bernardi, 1999). Furthermore, the open probability of the uniporter Ca^{2+} channel is nearly unity at normal $\Delta\Psi_m$ (Kirichok et al., 2004). It has been assumed that continuous Ca^{2+} extrusion compensates for influx (Nicholls, 2005) or, more commonly, that the low apparent Ca^{2+} affinity of the uniporter Ca^{2+} uptake mechanism effectively offsets this driving force (Carafoli, 1987; Drago et al., 2011; Nicholls, 2005; Rizzuto et al., 2004), but our results suggest that neither is the case. Addition of Ru360 in control cells did not unmask ongoing Ca^{2+} extrusion (Figure 2F), suggesting that Ca^{2+} influx is not constitutive under basal conditions. In contrast, Ru360 addition revealed ongoing Ca^{2+} extrusion in MICU1 KD cells, indicating that MCU-mediated Ca^{2+} uptake is activated and compensated for at a new higher steady-state $[Ca^{2+}]_m$ by constitutive Ca^{2+} extrusion that remains intact in MICU1 KD cells (Figure 2F and 2G). Studies of isolated mitochondria have suggested that $[Ca^{2+}]$ required for half-maximal uptake rate is up to 70 μM, with most estimates suggesting an apparent Ca^{2+} affinity of ~10 μM, or 100-fold higher than resting $[Ca^{2+}]_i$ (Bernardi, 1999; Gunter and Pfeiffer, 1990). We confirmed the low apparent affinity of MCU-mediated Ca^{2+} uptake, in the 10 μM range, although IMM depolarization by $[Ca^{2+}] > 20$ μM limits the ability to estimate this well, suggesting that 10 μM is a lower limit. Nevertheless, mitochondria in MICU1 KD cells accumulated Ca^{2+} at normal $\Delta\Psi_m$ from the cytoplasm where $[Ca^{2+}] = 70$ nM. Importantly therefore, the low apparent Ca^{2+} affinity of the uniporter does not effectively counteract the thermodynamic driving force. Accordingly, cells require regulatory mechanisms to limit MCU-mediated Ca^{2+} uptake under normal resting conditions. The results here suggest that MICU1 is an essential component of this mechanism.

Such mechanisms could operate by controlling kinetic properties of MCU-mediated Ca^{2+} uptake. However, MICU1 does not appear to utilize this strategy. The apparent V_{max}, K_d and Hill coefficient that describe the $[Ca^{2+}]$ dependence of MCU-mediated Ca^{2+} uptake are essentially identical in control and MICU1 KD cells. It was previously speculated that MICU1 might contribute to Ca^{2+} cooperativity of uniporter-mediated Ca^{2+} uptake (Perocchi et al., 2010), but our results suggest that the cooperativity is not mediated by MICU1 and resides elsewhere, possibly the MCU channel itself. Our results suggest instead that MICU1 acts as a Ca^{2+} sensor that sets a threshold $[Ca^{2+}]$ for $Ca^{2+}{}_m$ uptake. The $[Ca^{2+}]_i$ threshold for mitochondria that had not been pre-loaded with Ca^{2+} appears to be ~3 μM. This value was suggested by the steady-state bath $[Ca^{2+}]$ achieved by $[Ca^{2+}]_m$ uptake following exposure to boluses of Ca^{2+} or to slow rises in Ca^{2+} caused by ER Ca^{2+} leak. Below 3–4 μM Ca^{2+}, MCU-mediated Ca^{2+} uptake is strongly inhibited by MICU1.

The mechanism by which MICU1 inhibits MCU activity at $[Ca^{2+}]_i < ~3$ μM remains to be determined. MICU1 biochemically interacts with MCU (Figure S3A and (Baughman et al., 2011)), suggesting that MICU1 might regulate MCU activity directly, perhaps by acting as an endogenous ligand that blocks the permeation pathway or by altering MCU channel gating. Failure to rescue enhanced Ca^{2+} uptake in MICU1 KD cells with MICU1 containing disabling mutations in either Ca^{2+}-binding EF hand suggests that MICU1 plays an important role as a Ca^{2+} sensor in the mechanism. The requirement for two functional EF hands is consistent with MICU1 binding Ca^{2+} with high affinity (Gifford et al., 2007), as required for it to operate in the low $[Ca^{2+}]$ regime as observed. Our results suggest that the EF hands of

MICU1 are bound to Ca^{2+} under both $[Ca^{2+}]_i$ and $[Ca^{2+}]_m$ resting conditions, and this enables MICU1 to function as a brake to limit Ca^{2+} permeation through MCU. However, the lack of effect of MICU1, with or without functional EF hands, on the kinetic properties of MCU suggests that high $[Ca^{2+}]_m$ can overcome this block. Whether high $[Ca^{2+}]_m$ suppresses MICU1 inhibition by disrupting the physical interaction between MICU1 and MCU (not supported by preliminary data), or by other MCU-intrinsic or -extrinsic Ca^{2+} regulatory mechanisms remain to be determined.

A ruthenium-red sensitive $[Ca^{2+}]_m$uptake mode referred to as the “rapid mode”, or RaM, describes a phenomenon observed in isolated mitochondria in which Ca^{2+} uptake during the initial 300 msec of a Ca^{2+} pulse is much faster than the subsequent rate (Gunter et al., 2004; Sparagna et al., 1995). Of note, RaM was not observed in cases where mitochondria had been pre-incubated with ~150 nM bath Ca^{2+} (Buntinas et al., 2001; Gunter et al., 2004). The identification here of MICU1 as a high-affinity Ca^{2+} brake on MCU-mediated Ca^{2+} uptake may account for these observations. Thus, in mitochondria incubated in Ca^{2+}-depleted media, Ca^{2+} likely unbinds from MICU1, relieving inhibition of MCU. Upon addition of Ca^{2+}, uninhibited MCU would initially take up Ca^{2+} at a rapid rate until Ca^{2+} permeation into the matrix, shown to occur < 100 msec after a Ca^{2+} pulse (Gunter et al., 2004; Sparagna et al., 1995; Territo et al., 2001), enables $[Ca^{2+}]_m$ to reach levels for Ca^{2+} binding to the EF hands, triggering MICU1-mediated rapid inhibition of influx. In this model, the inability to observe RaM when mitochondria are incubated in 150 nM $Ca^{2+}$is due to matrix $[Ca^{2+}]$ being sufficiently high to ensure Ca^{2+} occupancy of the EF hands, enabling MICU1 to exert its normal inhibition of Ca^{2+} uptake.

Functional Implications of the Role of MICU1

$Ca^{2+}{}_m$ uptake regulates cell bioenergetics, physiological ROS signaling and $[Ca^{2+}]_i$ signals. Excessive $Ca^{2+}{}_m$ uptake can have deleterious effects, including inner membrane depolarization, mROS overproduction, sensitization to apoptotic and necrotic stimuli, and activation of the permeability transition pore and subsequent cell death pathways (see Introduction for references). Our results here demonstrate an essential role of MICU1 to control $Ca^{2+}{}_m$ uptake and protect cells against deleterious consequences associated with $Ca^{2+}{}_m$ overload. In the absence of MICU1, excessive MCU-mediated Ca^{2+} uptake led to elevated $[Ca^{2+}]_m$ under basal conditions and mROS overproduction and sensitivity to apoptotic stimuli. Physiologically-controlled delivery of Ca^{2+} to mitochondria can stimulate cellular bioenergetics (Balaban, 2009; Denton and McCormack, 1980; Robb-Gaspers et al., 1998; Territo et al., 2000). Lack of this delivery, as shown here in response to knockdown of MCU, causes bioenergetic stress (Cardenas et al., 2010). Conversely, over-expression of MCU to promote excessive $Ca^{2+}{}_m$ uptake can potentiate ceramide-induced cell death (De Stefani et al., 2011). MICU1 KD similarly potentiated stress-induced cell death. Of note, antioxidants mitigated these effects. Low mROS levels are required to maintain normal cellular functions, whereas aberrant mROS production leads to oxidative stress that is associated with cellular damage that ultimately leads to cell loss and organ failure (Hamanaka and Chandel, 2010). Our results emphasize the critical role played by MICU1 in regulating the nature of Ca^{2+}-dependent mitochondrial oxidant signaling.

In summary, our study has identified an essential role of MICU1 as a gatekeeper that sets the $[Ca^{2+}]_i$ threshold without affecting the kinetic properties of MCU-mediated $Ca^{2+}{}_m$ uptake. This essential regulation protects cells from $Ca^{2+}{}_m$ overload and consequent deleterious stress. The interaction between MICU1 and MCU may be an important target for cellular regulation that tunes $Ca^{2+}{}_m$ uptake to regulate bioenergetics and $[Ca^{2+}]_i$ and oxidant signaling in physiological and pathophysiological situations.

EXPERIMENTAL PROCEDURES

Cell Lines

Cells were grown Dulbecco's modified Eagle's medium supplemented (DMEM) supplemented with 10% FBS, 100 U/ml penicillin, and 100 μg/ml streptomycin at 37ºC, 5% CO_2. Details can be found in Extended Experimental Procedures. Endothelial cells were grown in endothelial cell growth supplement (ECGS) supplemented condition.

RNA Interference

HeLa, HEK-293 or endothelial cells were transfected with pools of distinct proprietary siRNAs and used 72 hr post-transfection unless otherwise stated. Details can be found in Extended Experimental Procedures.

Generation of Stable MICU1 Knockdown Cell Lines

Cells were transduced with MICU1 shRNA lentiviruses. Knockdown was assessed by qRT-PCR. Details can be found in Extended Experimental Procedures.

MICU1 Rescue Cells

MICU1 rescues were created by expressing constructs resistant to MICU1 shRNA knockdown. Details can be found in Extended Experimental Procedures.

qRT–PCR Analysis

Total RNA was isolated from cells using RNAesy Minikit (Qiagen) and total RNA was reverse transcribed. Quantitative Real-time PCR reactions were performed with gene specific primers. Details can be found in Extended Experimental Procedures.

Simultaneous Measurement of Cytoplasmic and Mitochondrial Ca^{2+} Concentrations ($[Ca^{2+}]_c$ and $[Ca^{2+}]_m$)

Cells grown on 25-mm glass coverslips were loaded with 2 μM rhod-2/AM (50 min) and 5 μM Fluo-4/AM (30 min) in extracellular medium as previously described (Madesh et al., 2005). Coverslips were mounted in an open perfusion microincubator (PDMI-2; Harvard Apparatus) at 37°C and imaged. After 1 min of baseline recording, histamine (100 μM) was added and confocal images were recorded every 3 s (510 Meta; Carl Zeiss, Inc.) at 488- and 561-nm excitation using a 63× oil objective. Images were analyzed and quantitated using ImageJ (NIH) (Hawkins et al., 2010; Madesh et al., 2005; Mallilankaraman et al., 2011).

Simultaneous Measurement of Ca^{2+} Uptake and Mitochondrial Membrane Potential ($\Delta\Psi_m$) in Permeabilized Cells

Negative shRNA, MICU1 KD, MICU1 Rescue, MICU1 EF1 mutant and MICU1 EF2 mutant cells were trypsinized, counted (6×10^6) and washed in an extracellular-like Ca^{2+}-free buffer (in mM: 120 NaCl, 5 KCl, 1 KH_2PO_4, 0.2 $MgCl_2$, 0.1 EGTA, and 20 HEPES-NaOH, pH 7.4). Following centrifugation, cells were transferred to an intracellular-like medium (permeabilization buffer, in mM: 120 KCl, 10 NaCl, 1 KH_2PO_4, 20 HEPES-Tris, pH 7.2, protease inhibitors (EDTA-free complete™ tablets, Roche Applied Science), 2 μM thapsigargin and digitonin (40 μg/ml)). The cell suspension supplemented with succinate (2 mM) was placed in a fluorimeter and permeabilized by gentle stirring. FuraFF (0.5 μM) was added at 0 s and JC-1 (800 nm) at 20 s to simultaneously measure extra-mitochondrial $Ca^{2+}$and $\Delta\Psi_m$. Fluorescence was monitored in a temperature-controlled (37ºC) multi-wavelength-excitation dual wavelength-emission spectrofluorometer (Delta RAM, Photon Technology International) using 490-nm excitation/535-nm emission for the monomer, 570-

nm excitation/595-nm emission for the J-aggregate of JC1and 340-nm/380-nm for FuraFF. The ratiometric dye, FuraFF was calibrated as previously described. At 450 s, Ca^{2+}pulses were added and $\Delta\Psi_m$ and extra-mitochondrial Ca^{2+} were monitored simultaneously. CCCP was added at 750 s to determine mitochondrial Ca^{2+} content.

Mitochondrial Ca^{2+} uptake rate was derived by fitting the decay of bath $[Ca^{2+}]$ after a Ca^{2+} pulse to the equation: $y=y_0+A\exp(-[t-t_0]/\tau)$, where A is the change in bath $[Ca^{2+}]$ between the peak and the decay asymptote and τ is the decay time constant. Ca^{2+} uptake rate (A/τ) as a function of extra-mitochondrial calcium, $[Ca^{2+}]_{out}$, was fitted (Igor Pro 6.2) to a Hill equation to derive kinetic parameters of MCU-mediated Ca^{2+} uptake:

Ca^{2+} uptake rate $= V_{max}/\left[1+\left(K_{act}/\left[Ca^{2+}\right]\right)^{H}\right]$, where V_{max} is the maximum rate, K_{act} the half-maximal bath $[Ca^{2+}]$, and H is the Hill coefficient. The total amount of Ca^{2+} accumulated by MCU-mediated Ca^{2+} uptake (mitochondrial Ca^{2+} buffering capacity) was evaluated by measuring the change in bath $[Ca^{2+}]$ in response to the uncoupler CCCP. MCU-mediated Ca^{2+} accumulation as a function of extra-mitochondrial $[Ca^{2+}]$ was fitted (Origin 7.0) with a 3-parameter model: $y = a - b\ln(x + c)$.

Immunoprecipitation

Transfected cells were harvested and lysed. Anti-Flag agarose beads (Novus) were used for immunoprecipitation. Anti-GFP (Cell Signaling) was used to detect MCU. Details can be found in Extended Experimental Procedures.

Western Blotting and Treatments

Standard techniques were used. Chemiluminescence detection was performed at exposures within the linear range. Details can be found in Extended Experimental Procedures.

Oxygen Consumption

Oxygen consumption rate (OCR) was measured at 37°C using XF24 extracellular analyzer (Seahorse Bioscience) as described (Cardenas et al., 2010). Details can be found in Extended Experimental Procedures.

Measurement of Mitochondrial Superoxide (mROS)

Mitochondrial superoxide was measured using the mitochondrial $O_2^{\bullet-}$ indicator MitoSOX Red (Molecular probes; Invitrogen) as described (Mallilankaraman et al., 2011; Mukhopadhyay et al., 2007). Briefly, cells grown on coated glass coverslips were loaded with 5 μM MitoSOX Red for 30 min, coverslips were mounted in an open perfusion microincubator (PDMI-2; Harvard Apparatus) at 37°C and imaged. Confocal (510 Meta; Carl Zeiss, Inc.) images were obtained at 561-nm excitation using a 63× oil objective. For DPI treatment, cells were incubated with 30 μM DPI for 30 min prior to dye loading. For Antimycin A treatment, cells were incubated with 2 μM Antimycin A for 30 min prior to dye loading. Images were analyzed and the mean MitoSOX Red fluorescence was quantified using Image J software (NIH).

Cell Proliferation Assay

Cell proliferation was measured using the Cell Trace™ CFSE Cell proliferation Kit (Molecular Probes, Invitrogen). Details can be found in Extended Experimental Procedures.

Migration Assay

To assess endothelial cell migration, a scratch assay was employed, as described in Extended Experimental Procedures.

Cell Death Assay

Cell death was evaluated with the Aqua LIVE/DEAD® Fixable Dead Cell Stain kit (Molecular Probes, Invitrogen). Details can be found in Extended Experimental Procedures.

Flow Cytometry

Details can be found in Extended Experimental Procedures.

Luciferase Assay

Cells were transfected with NFAT-luciferase reporter plasmids and luciferase activity was detected using Bright-Glo™ Luciferase Assay System (Promega). Details can be found in Extended Experimental Procedures.

NFAT Nuclear Translocation

Cells were transduced with Ad5-NFATC3-GFP. Confocal images were acquired and nuclear translocation was assessed by counting the number of nuclear-GFP positive cells. Details can be found in Extended Experimental Procedures.

Statistical Analyses

Unless indicated, all experiments were repeated thrice and recordings are representative of the mean fluorescence value of all cells/field or parameter. Data from multiple experiments were quantified to determine peak n-fold or percent change, expressed as mean ± S.E. and differences between groups were analyzed using 2-tailed Student's t test or, when not normally distributed, a Mann-Whitney U test. Differences in means among multiple data sets were analyzed using 1-way ANOVA with the Kruskal-Wallis test, followed by pairwise comparison using the Dunn test. P value < 0.05 was considered significant in all analyses. Data were computed either with Graphpad Prism version 5.0 or SigmaPlot Software.

Supplementary Material

Refer to Web version on PubMed Central for supplementary material.

Acknowledgments

Supported by NIH grants HL086699, HL086699-01A2S1 and 1S10RR027327-01 to MM, and GM56328 and MH059937 to J.K.F. We thank Jun Yang for biochemistry assistance and the University of Pennsylvania IDOM (P30-DK19535) for assistance. C.C. was supported by the American Heart Association. R.M. was supported by an NRSA Fellowship.

References

Azzone GF, Bragadin M, Pozzan T, Antone PD. Proton electrochemical potential in steady state rat liver mitochondria. Biochim Biophys Acta. 1977; 459:96–109. [PubMed: 12814]

Balaban RS. The role of Ca^{2+} signaling in the coordination of mitochondrial ATP production with cardiac work. Biochim Biophys Acta. 2009; 1787:1334–1341. [PubMed: 19481532]

Balaban RS, Nemoto S, Finkel T. Mitochondria, oxidants, and aging. Cell. 2005; 120:483–495. [PubMed: 15734681]

Baughman JM, Perocchi F, Girgis HS, Plovanich M, Belcher-Timme CA, Sancak Y, Bao XR, Strittmatter L, Goldberger O, Bogorad RL, et al. Integrative genomics identifies MCU as an essential component of the mitochondrial calcium uniporter. Nature. 2011; 476:341–345. [PubMed: 21685886]

Bernardi P. Mitochondrial transport of cations: channels, exchangers, and permeability transition. Physiol Rev. 1999; 79:1127–1155. [PubMed: 10508231]

Bragadin M, Pozzan T, Azzone GF. Kinetics of Ca^{2+} carrier in rat liver mitochondria. Biochemistry. 1979; 18:5972–5978. [PubMed: 42437]

Buntinas L, Gunter KK, Sparagna GC, Gunter TE. The rapid mode of calcium uptake into heart mitochondria (RaM): comparison to RaM in liver mitochondria. Biochim Biophys Acta. 2001; 1504:248–261. [PubMed: 11245789]

Carafoli E. Intracellular calcium homeostasis. Annu Rev Biochem. 1987; 56:395–433. [PubMed: 3304139]

Carafoli E, Lehninger AL. A survey of the interaction of calcium ions with mitochondria from different tissues and species. Biochem J. 1971; 122:681–690. [PubMed: 5129264]

Cardenas C, Miller RA, Smith I, Bui T, Molgo J, Muller M, Vais H, Cheung KH, Yang J, Parker I, et al. Essential regulation of cell bioenergetics by constitutive $InsP_3$ receptor Ca^{2+} transfer to mitochondria. Cell. 2010; 142:270–283. [PubMed: 20655468]

Collins TJ, Lipp P, Berridge MJ, Bootman MD. Mitochondrial Ca^{2+} uptake depends on the spatial and temporal profile of cytosolic Ca^{2+} signals. J Biol Chem. 2001; 276:26411–26420. [PubMed: 11333261]

De Stefani D, Raffaello A, Teardo E, Szabo I, Rizzuto R. A forty-kilodalton protein of the inner membrane is the mitochondrial calcium uniporter. Nature. 2011; 476:336–340. [PubMed: 21685888]

Denton RM, McCormack JG. The role of calcium in the regulation of mitochondrial metabolism. Biochem Soc Trans. 1980; 8:266–268. [PubMed: 7399049]

Drago I, Pizzo P, Pozzan T. After half a century mitochondrial calcium in- and efflux machineries reveal themselves. EMBO J. 2011; 30:4119–4125. [PubMed: 21934651]

Duchen MR, Verkhratsky A, Muallem S. Mitochondria and calcium in health and disease. Cell Calcium. 2008; 44:1–5. [PubMed: 18378306]

Filippin L, Magalhaes PJ, Di Benedetto G, Colella M, Pozzan T. Stable interactions between mitochondria and endoplasmic reticulum allow rapid accumulation of calcium in a subpopulation of mitochondria. J Biol Chem. 2003; 278:39224–39234. [PubMed: 12874292]

Gifford JL, Walsh MP, Vogel HJ. Structures and metal-ion-binding properties of the Ca^{2+}-binding helix-loop-helix EF-hand motifs. Biochem J. 2007; 405:199–221. [PubMed: 17590154]

Gunter KK, Gunter TE. Transport of calcium by mitochondria. J Bioenerg Biomembr. 1994; 26:471–485. [PubMed: 7896763]

Gunter TE, Gunter KK, Sheu SS, Gavin CE. Mitochondrial calcium transport: physiological and pathological relevance. Am J Physiol. 1994; 267:C313–339. [PubMed: 8074170]

Gunter TE, Pfeiffer DR. Mechanisms by which mitochondria transport calcium. Am J Physiol. 1990; 258:C755–786. [PubMed: 2185657]

Gunter TE, Yule DI, Gunter KK, Eliseev RA, Salter JD. Calcium and mitochondria. FEBS Lett. 2004; 567:96–102. [PubMed: 15165900]

Hajnoczky G, Robb-Gaspers LD, Seitz MB, Thomas AP. Decoding of cytosolic calcium oscillations in the mitochondria. Cell. 1995; 82:415–424. [PubMed: 7634331]

Hamanaka RB, Chandel NS. Mitochondrial reactive oxygen species regulate cellular signaling and dictate biological outcomes. Trends Biochem Sci. 2010; 35:505–513. [PubMed: 20430626]

Hansford RG. Physiological role of mitochondrial Ca^{2+} transport. J Bioenerg Biomembr. 1994; 26:495–508. [PubMed: 7896765]

Hawkins BJ, Irrinki KM, Mallilankaraman K, Lien YC, Wang Y, Bhanumathy CD, Subbiah R, Ritchie MF, Soboloff J, Baba Y, et al. S-glutathionylation activates STIM1 and alters mitochondrial homeostasis. J Cell Biol. 2010; 190:391–405. [PubMed: 20679432]

Herrington J, Park YB, Babcock DF, Hille B. Dominant role of mitochondria in clearance of large Ca^{2+} loads from rat adrenal chromaffin cells. Neuron. 1996; 16:219–228. [PubMed: 8562086]

Hoth M, Button DC, Lewis RS. Mitochondrial control of calcium-channel gating: a mechanism for sustained signaling and transcriptional activation in T lymphocytes. Proc Natl Acad Sci U S A. 2000; 97:10607–10612. [PubMed: 10973476]

Igbavboa U, Pfeiffer DR. EGTA inhibits reverse uniport-dependent Ca^{2+} release from uncoupled mitochondria. Possible regulation of the Ca^{2+} uniporter by a Ca^{2+} binding site on the cytoplasmic side of the inner membrane. J Biol Chem. 1988; 263:1405–1412. [PubMed: 2447088]

Jacobson J, Duchen MR. Mitochondrial oxidative stress and cell death in astrocytes--requirement for stored Ca^{2+} and sustained opening of the permeability transition pore. J Cell Sci. 2002; 115:1175–1188. [PubMed: 11884517]

Kirichok Y, Krapivinsky G, Clapham DE. The mitochondrial calcium uniporter is a highly selective ion channel. Nature. 2004; 427:360–364. [PubMed: 14737170]

Lambeth JD. NOX enzymes and the biology of reactive oxygen. Nat Rev Immunol. 2004; 4:181–189. [PubMed: 15039755]

Lemasters JJ, Theruvath TP, Zhong Z, Nieminen AL. Mitochondrial calcium and the permeability transition in cell death. Biochim Biophys Acta. 2009; 1787:1395–1401. [PubMed: 19576166]

Madesh M, Hawkins BJ, Milovanova T, Bhanumathy CD, Joseph SK, Ramachandrarao SP, Sharma K, Kurosaki T, Fisher AB. Selective role for superoxide in $InsP_3$ receptor-mediated mitochondrial dysfunction and endothelial apoptosis. J Cell Biol. 2005; 170:1079–1090. [PubMed: 16186254]

Mallilankaraman K, Gandhirajan RK, Hawkins BJ, Madesh M. Visualization of vascular Ca2+ signaling triggered by paracrine derived ROS. J Vis Exp. 2011

McCormack JG, Halestrap AP, Denton RM. Role of calcium ions in regulation of mammalian intramitochondrial metabolism. Physiol Rev. 1990; 70:391–425. [PubMed: 2157230]

Mukhopadhyay P, Rajesh M, Hasko G, Hawkins BJ, Madesh M, Pacher P. Simultaneous detection of apoptosis and mitochondrial superoxide production in live cells by flow cytometry and confocal microscopy. Nat Protoc. 2007; 2:2295–2301. [PubMed: 17853886]

Nicholls DG. The regulation of extramitochondrial free calcium ion concentration by rat liver mitochondria. Biochem J. 1978; 176:463–474. [PubMed: 33670]

Nicholls DG. Mitochondria and calcium signaling. Cell Calcium. 2005; 38:311–317. [PubMed: 16087232]

Nicholls DG. Forty years of Mitchell's proton circuit: From little grey books to little grey cells. Biochim Biophys Acta. 2008; 1777:550–556. [PubMed: 18423395]

O'Rourke B. Mitochondrial ion channels. Annu Rev Physiol. 2007; 69:19–49. [PubMed: 17059356]

Orrenius S, Zhivotovsky B, Nicotera P. Regulation of cell death: the calcium-apoptosis link. Nat Rev Mol Cell Biol. 2003; 4:552–565. [PubMed: 12838338]

Palmer AE, Giacomello M, Kortemme T, Hires SA, Lev-Ram V, Baker D, Tsien RY. Ca^{2+} indicators based on computationally redesigned calmodulin-peptide pairs. Chem Biol. 2006; 13:521–530. [PubMed: 16720273]

Perocchi F, Gohil VM, Girgis HS, Bao XR, McCombs JE, Palmer AE, Mootha VK. MICU1 encodes a mitochondrial EF hand protein required for Ca^{2+} uptake. Nature. 2010; 467:291–296. [PubMed: 20693986]

Rizzuto R, Duchen MR, Pozzan T. Flirting in little space: the ER/mitochondria Ca^{2+} liaison. Sci STKE. 2004:re1. [PubMed: 14722345]

Rizzuto R, Pinton P, Carrington W, Fay FS, Fogarty KE, Lifshitz LM, Tuft RA, Pozzan T. Close contacts with the endoplasmic reticulum as determinants of mitochondrial Ca^{2+} responses. Science. 1998; 280:1763–1766. [PubMed: 9624056]

Robb-Gaspers LD, Burnett P, Rutter GA, Denton RM, Rizzuto R, Thomas AP. Integrating cytosolic calcium signals into mitochondrial metabolic responses. EMBO J. 1998; 17:4987–5000. [PubMed: 9724635]

Rottenberg H, Scarpa A. Calcium uptake and membrane potential in mitochondria. Biochemistry. 1974; 13:4811–4817. [PubMed: 4429666]

Santo-Domingo J, Demaurex N. Calcium uptake mechanisms of mitochondria. Biochim Biophys Acta. 2010; 1797:907–912. [PubMed: 20079335]

Simpson PB, Russell JT. Mitochondrial Ca^{2+} uptake and release influence metabotropic and ionotropic cytosolic Ca^{2+} responses in rat oligodendrocyte progenitors. J Physiol. 1998; 508(Pt 2): 413–426. [PubMed: 9508806]

Sparagna GC, Gunter KK, Sheu SS, Gunter TE. Mitochondrial calcium uptake from physiological-type pulses of calcium. A description of the rapid uptake mode. J Biol Chem. 1995; 270:27510–27515. [PubMed: 7499209]

Spat A, Szanda G, Csordas G, Hajnoczky G. High- and low-calcium-dependent mechanisms of mitochondrial calcium signalling. Cell Calcium. 2008; 44:51–63. [PubMed: 18242694]

Szalai G, Krishnamurthy R, Hajnoczky G. Apoptosis driven by IP(3)-linked mitochondrial calcium signals. EMBO J. 1999; 18:6349–6361. [PubMed: 10562547]

Territo PR, French SA, Dunleavy MC, Evans FJ, Balaban RS. Calcium activation of heart mitochondrial oxidative phosphorylation: rapid kinetics of mVO2, NADH, AND light scattering. J Biol Chem. 2001; 276:2586–2599. [PubMed: 11029457]

Territo PR, Mootha VK, French SA, Balaban RS. Ca^{2+} activation of heart mitochondrial oxidative phosphorylation: role of the F(0)/F(1)-ATPase. Am J Physiol Cell Physiol. 2000; 278:C423–435. [PubMed: 10666039]

Article highlights

- MICU1 inhibits the mitochondrial Ca^{2+} channel MCU under resting conditions
- MICU1 sets a cytoplasmic Ca^{2+} concentration threshold for mitochondrial Ca^{2+} uptake
- Loss of MICU1 results in mitochondrial Ca^{2+} overload
- Mitochondrial Ca^{2+} overload causes excessive ROS production and cell stress

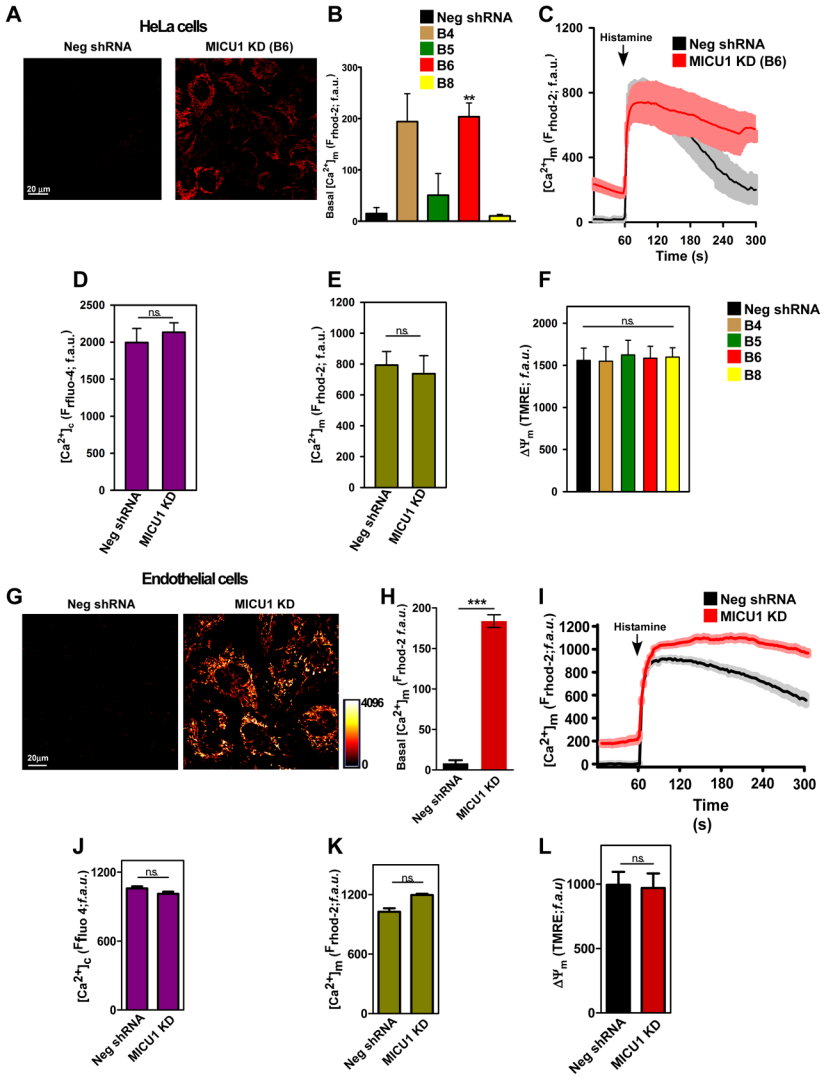

Figure 1. MICU1 Silencing Promotes Basal Ca^{2+}_m Accumulation

(A) Representative confocal images of rhod-2 fluorescence in HeLa Neg shRNA (control) and MICU1 shRNA clone KD #B6 cells.

(B) Quantification of basal rhod-2 fluorescence in HeLa Neg shRNA (control) and MICU1 shRNA KD clones. Mean ± SEM.; ns, not significant; **: $P < 0.01$, n=3.

(C) Kinetics of Ca^{2+}_m in HeLa Neg shRNA (control) and MICU1 shRNA KD clone #B6 cells in response to histamine (100 μM). Solid lines: mean; shaded regions: ± SEM.; n=3.

(D) and (E) Quantification of cytosolic (purple) and mitochondrial (green) $[Ca^{2+}]$ peak amplitudes in HeLa Neg shRNA (control) and MICU1 shRNA KD clone #B6 cells after stimulation with 100 μM histamine. Mean ± SEM.; n=3.

(F) Quantification of TMRE fluorescence to assess ΔΨm in HeLa Neg shRNA (control) and MICU1 shRNA KD clones. Mean ± SEM.; n=3. See also Figure S1.

(G) Representative confocal images of rhod-2 fluorescence in Neg shRNA (control) and MICU1 shRNA clone KD #B6 ECs.

(H) Quantification of basal rhod-2 fluorescence in Neg shRNA (control) and MICU1 KD ECs. Mean ± SEM.; **: $P < 0.01$, n=3.

(I) Kinetics of Ca^{2+}_m in Neg shRNA (control) and MICU1 KD ECs in response to histamine (100 μM). Solid lines: mean; shaded regions: ± SEM; n=3.

(J) and (K) Quantification of cytosolic (purple) and mitochondrial (green) [Ca^{2+}] peak amplitudes in Neg shRNA (control) and MICU1 KD ECs after stimulation with histamine (100 μM). Mean ± SEM.; n=3.
(L) Quantification of TMRE fluorescence to assess ΔΨm in Neg shRNA (control) and MICU1 shRNA KD #B6 ECs. Mean ± SEM; n=3.

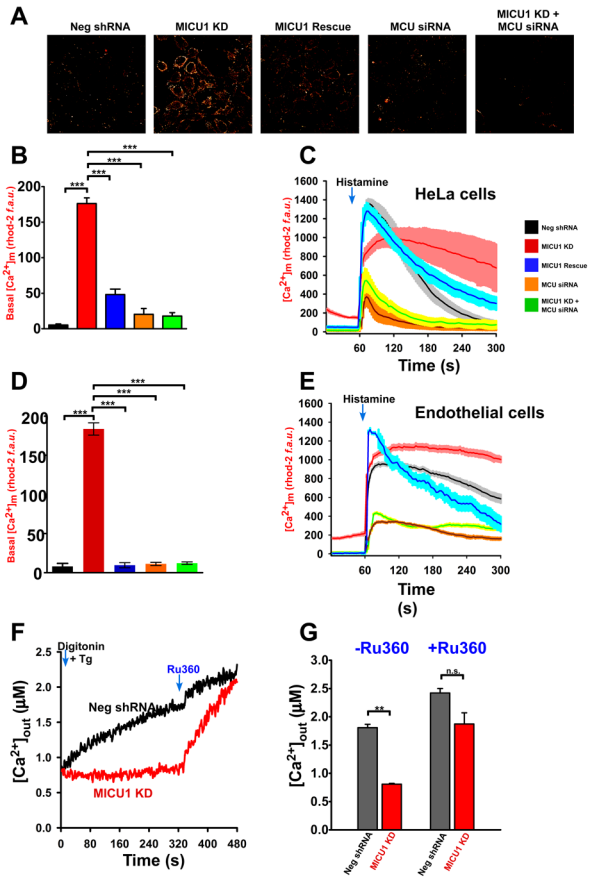

Figure 2. MICU1 Knockdown-Induced Basal Ca^{2+}_m Accumulation is Mediated by MCU-Dependent Ca^{2+} Uptake

(A) Representative confocal images of basal rhod-2 fluorescence in HeLa cells stably expressing Neg shRNA, MICU1 KD shRNA and MICU1 Rescue, and WT cells treated with MCU siRNA and MICU1 KD cells treated with MCU siRNA.

(B) Quantification of basal rhod-2 fluorescence of cells in (A). Mean ± SEM; ***: P < 0.001, n=3.

(C) Responses of Ca^{2+}_m in cells in (A) to 100 μM histamine. Solid lines: mean; shaded regions: ± SEM; n=3.

(D) Quantification of basal rhod-2 fluorescence in ECs stably expressing Neg shRNA, MICU1 KD shRNA and MICU1 Rescue, and WT cells treated with MCU siRNA and MICU1 KD cells treated with MCU siRNA. Mean ± SEM; ***: P < 0.001, n=3.

(E) Responses of Ca^{2+}_m in ECs in (D) to 100 μM histamine. Solid lines: mean; shaded regions: ± SEM; n=3.

(F) and (G) Representative traces and quantification of basal bath $[Ca^{2+}]$ (Fura FF fluorescence) in Neg shRNA (black) and MICU1KD (red) permeabilized HEK293 cells before and after Ru360. Mean ± SEM; ns, not different; **: P <0.01, n=3. See also Figure S2

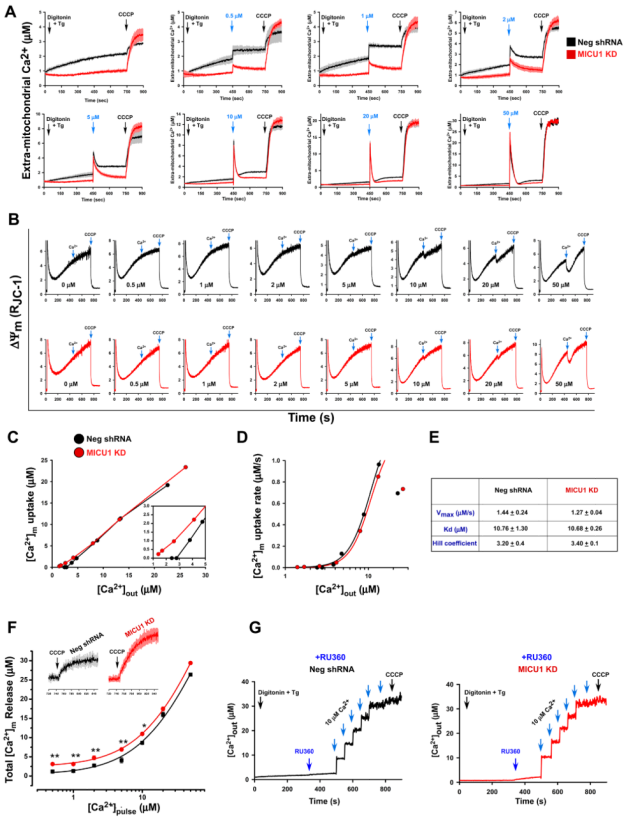

Figure 3. MICU1 Controls MCU-Mediated Ca^{2+}_m Uptake in Low $[Ca^{2+}]_i$

(A) Permeabilized stable Neg shRNA (black) and MICU1 KD (red) HEK293 cells were pulsed with different $[Ca^{2+}]$ as indicated. Traces show bath $[Ca^{2+}]$ (μM). Solid lines: mean; shaded regions: ± SEM; n=3.

(B) Representative traces indicate $\Delta\Psi_m$ (JC-1 ratio) in permeabilized Neg shRNA (black) and MICU1 KD (red) HEK293 cells in response to Ca^{2+} pulses and CCCP.

(C) Change in bath $[Ca^{2+}]$ due to Ca^{2+}_m uptake in response to various bath $[Ca^{2+}]$ in control (black) and MICU1 KD (red) cells. Uptake derived from single exponential fit of bath $[Ca^{2+}]$ kinetics following Ca^{2+} pulses. Inset shows responses up to 5 μM bath $[Ca^{2+}]$.

(D) Rate of $[Ca^{2+}]_m$ as function of bath $[Ca^{2+}]$ derived from single exponential fits of bath $[Ca^{2+}]$ responses following Ca^{2+} pulses. Solid line is Hill equation fit of data. Reduced uptake rate observed at $[Ca^{2+}] > 20$ μM is due to $\Delta\Psi$m depolarization, and was not used in fitting.

(E) Kinetic parameters derived from Hill equation fits of data in (C).

(F) Total Ca^{2+}_m uptake after each Ca^{2+} pulse was determined in neg shRNA (black) and MICU1 KD (red) cells by recording Ca^{2+} released by CCCP. Inset: Traces obtained from cells with no added Ca^{2+} pulse. Solid lines: mean; shaded regions: Mean ± SEM; n= 3. **, *: $P < 0.01$ and 0.05, respectively.

(G) Ru360 blocks basal Ca^{2+}_m uptake in MICU1 KD cells as well as uptake in KD and control cells in response to Ca^{2+} pulses. Representative traces from 3 experiments. See also Figure S3.

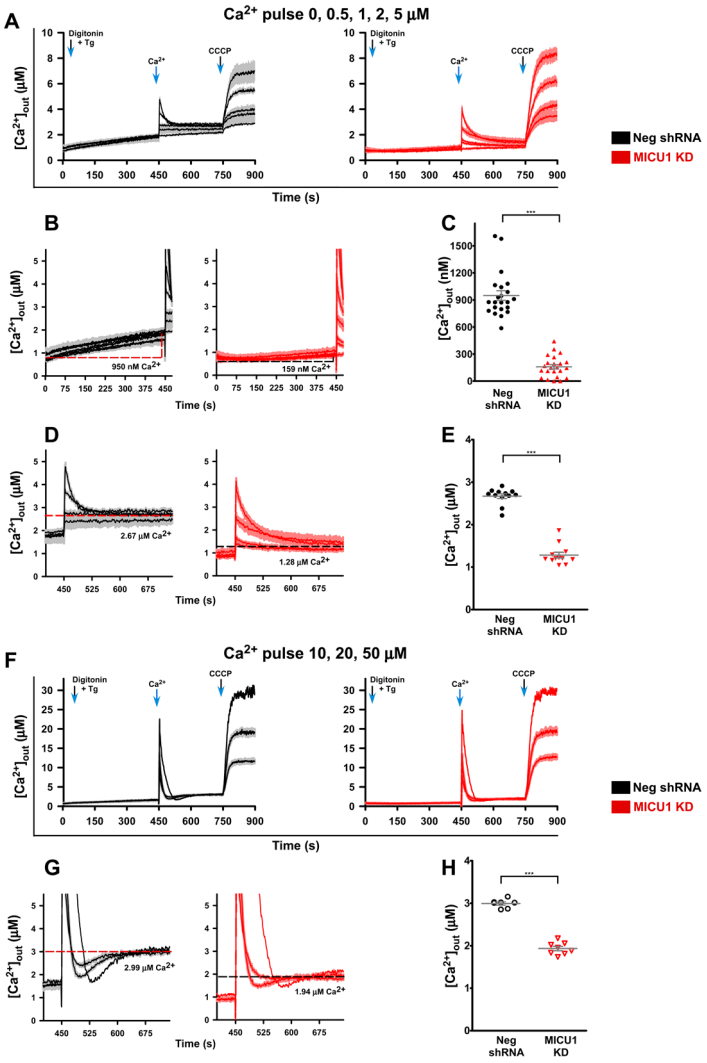

Figure 4. MICU1 Silencing Lowers the Set-Point for Basal MCU-Mediated Ca^{2+} Uptake

(A) Overlay of bath [Ca^{2+}] responses to 0, 0.5, 1, 2 and 5 μM Ca^{2+} pulses in permeabilized Neg shRNA (black; left panel) and MICU1 KD cells (red; right panel). Solid lines: means; shaded areas: Mean ± SEM; n=3 at each [Ca^{2+}].

(B) Overlay of bath [Ca^{2+}] kinetics during 450 sec following plasma membrane permeabilization and exposure to Tg in Neg shRNA control (black) and MICU1 KD (red) cells. Solid lines: means; shaded areas: Mean ± SEM; n=3 at each [Ca^{2+}].

(C) Scatter plot of bath [Ca^{2+}] at 450 sec from experiments shown in B. Mean ± SEM shown. ***, $P < 0.001$

(D) Overlay of bath [Ca^{2+}] kinetics during 300 sec following 0.5, 1, 2 and 5 μM bath Ca^{2+} pulses in permeabilized Neg shRNA (black; left panel) and MICU1 KD cells (red; right panel). Solid lines: means; shaded areas: Mean ± SEM; n=3 at each [Ca^{2+}].

(E) Scatter plot of bath [Ca^{2+}] at 300 sec from experiments shown in D. Mean ± SEM shown. ***, $P < 0.001$.

(F) Overlay of bath [Ca^{2+}] responses to 10, 20 and 50 μM Ca^{2+} pulses in permeabilized Neg shRNA (black; left panel) and MICU1 KD cells (red; right panel). Solid lines: means; shaded areas: Mean ± SEM; n=3 at each [Ca^{2+}].

(G) Overlay of bath [Ca^{2+}] kinetics during 300 sec following 10, 20 and 50 μM bath Ca^{2+} pulses in permeabilized Neg shRNA (black; left panel) and MICU1 KD cells (red; right panel). Solid lines: means; shaded areas: Mean ± SEM; n=3 at each [Ca^{2+}].
(H) Scatter plot of bath [Ca^{2+}] at 300 sec from experiments in (G). ***: $P < 0.001$ See also Figure S4

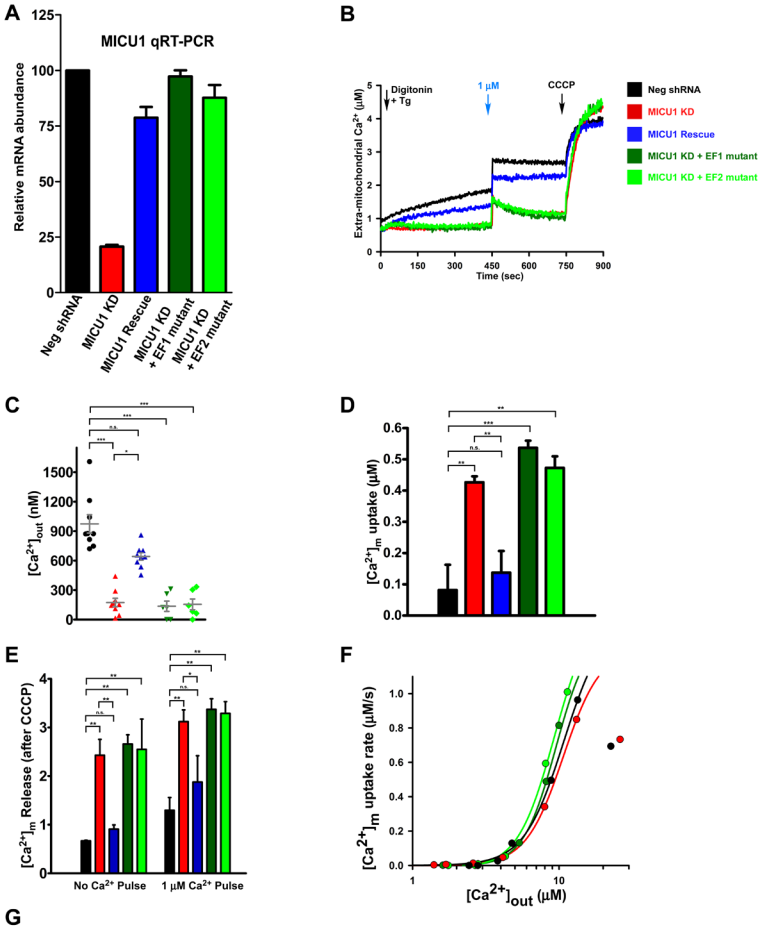

G

	Neg shRNA	MICU1 KD	MICU1 EF1 mutant	MICU1 EF2 mutant
V_{max} (μM/s)	1.44 ± 0.24	1.27 ± 0.04	1.45 ± 0.16	1.48 ± 0.23
Kd (μM)	10.76 ± 1.30	10.68 ± 0.26	9.77 ± 0.56	9.90 ± 0.89
Hill coefficient	3.20 ± 0.4	3.40 ± 0.1	3.76 ± 0.24	3.75 ± 0.73

Figure 5. EF Hand Domains of MICU1 Regulate the Ca^{2+} Threshold for MCU-Mediated Ca^{2+} Uptake

(A) Knockdown of MICU1 mRNA levels in HEK293 Neg shRNA, MICU1 KD, MICU1 Rescue, MICU1 KD stably expressing shRNA insensitive MICU1 cDNA harboring either D231A and E242K mutation (EF1 mutant) or D421A and E432K mutation (EF2 mutant) cells (mean ± SEM.; n=3).

(B) Permeabilized HEK293 Neg shRNA, MICU1 KD, MICU1 Rescue, MICU1 KD stably expressing shRNA insensitive MICU1 cDNA harboring either EF1 or EF2 mutations, cells were pulsed with 1 μM Ca^{2+} as indicated. Representative traces show bath [Ca^{2+}] (μM).

(C) Quantification of basal bath [Ca^{2+}] at 450 sec after permeabilization. *, **, ***: P < 0.05, 0.01, 0.001, respectively. Mean ± SEM; n=3.

(D) Change in bath [Ca^{2+}] due to $Ca^{2+}{}_m$ uptake in response to 1 μM Ca^{2+} pulse. Uptake derived from single exponential fit of bath [Ca^{2+}] kinetics following Ca^{2+} pulse. Mean ± S.E.; **, ***: P < 0.01 and 0.001, respectively. n.s. not significant. Mean ± SEM; n=3.

(E) Total $Ca^{2+}{}_m$ uptake after basal accumulation (no Ca^{2+} pulse) or 1 μM Ca^{2+} pulse determined by recording Ca^{2+} released by CCCP addition at t = 750 sec. Mean ± S.E.; *, **: P < 0.05 and 0.01, respectively. Mean ± SEM; n=3.

(F) Rate of Ca^{2+}_m uptake as function of bath [Ca^{2+}] derived from single exponential fits of bath [Ca^{2+}] responses following Ca^{2+} pulses in permeabilized EF1 or EF2 mutant cells. Solid line is Hill equation fit of the data. Reduced uptake rate observed at [Ca^{2+}] > 20 μM is due to ΔΨm depolarization, and was not used in the fitting.
(G) Kinetic parameters derived from Hill equation fits of data in (F). See also Figure S5.

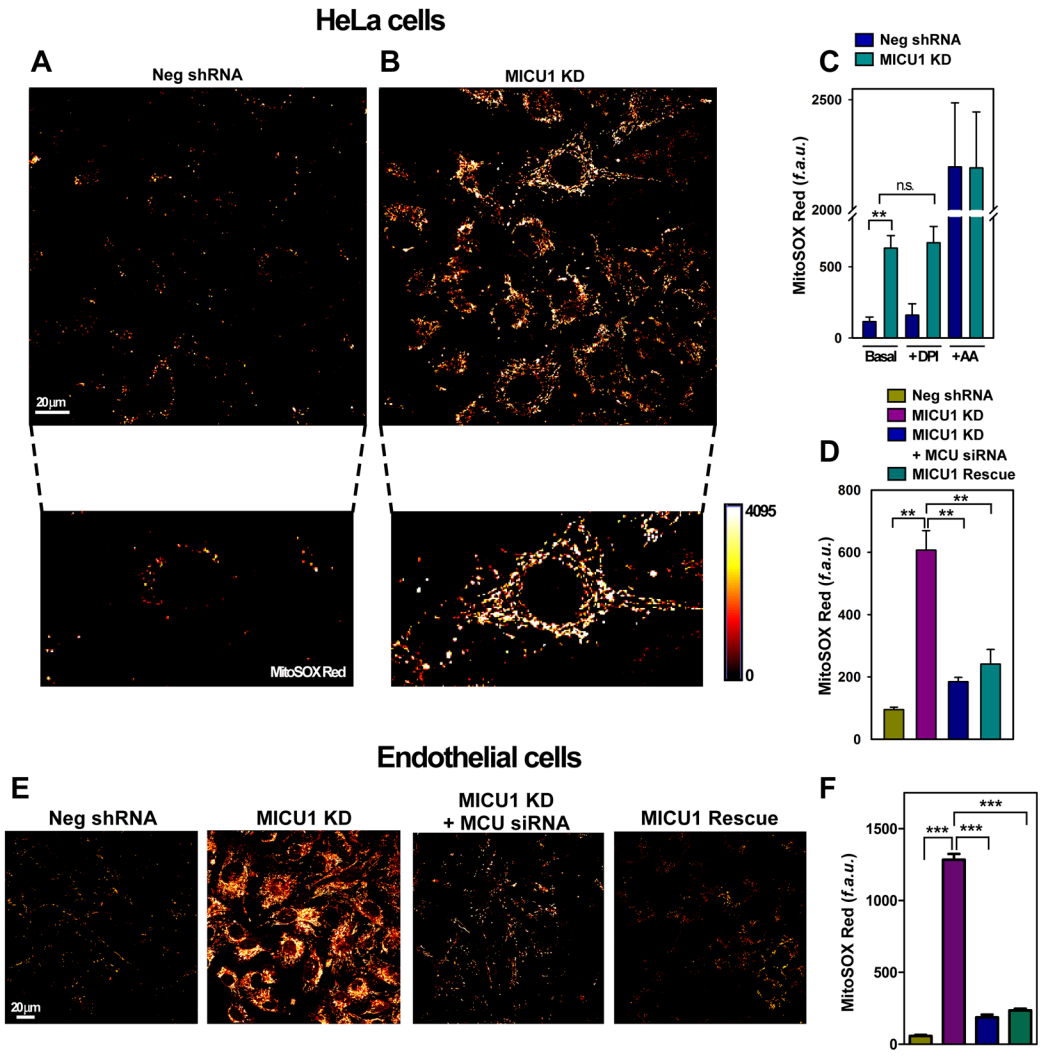

Figure 6. MICU1 Deficiency Elevates Basal Mitochondrial ROS

(A and B)Representative confocal images show MitoSOX Red fluorescence in Neg shRNA (A) and MICU1 KD (B) HeLa cells. Bottom panels: Enlarged portions of fields showing single cells depicting mitochondrial localization of indicator.

(C) Quantification of MitoSOX Red fluorescence in Neg shRNA and MICU1 KD cells, with or without NADPH oxidase inhibitor DPI (10 μM). Mitochondrial respiratory Complex III blocker antimycin A (AA) used as positive control. Mean ± SEM; **: P<0.01, ns, not different; n=3.

(D) Quantification of MitoSOX Red fluorescence in MICU1 KD, MCU siRNA treated MICU1 KD and MICU1 rescue HeLa cells. Mean ± SEM; **: P<0.01; n = 3.

(E)Representative confocal images of MitoSOX Red fluorescence in Neg shRNA, MICU1 KD, MICU1 KD +MCU siRNA and MICU1 rescue ECs.

(F) Quantification of MitoSOX Red fluorescence in MICU1 KD, MCU siRNA treated MICU1 KD and MICU1 rescue ECs. Mean ± SEM; **: P<0.01; n = 3. See also Figure S6.

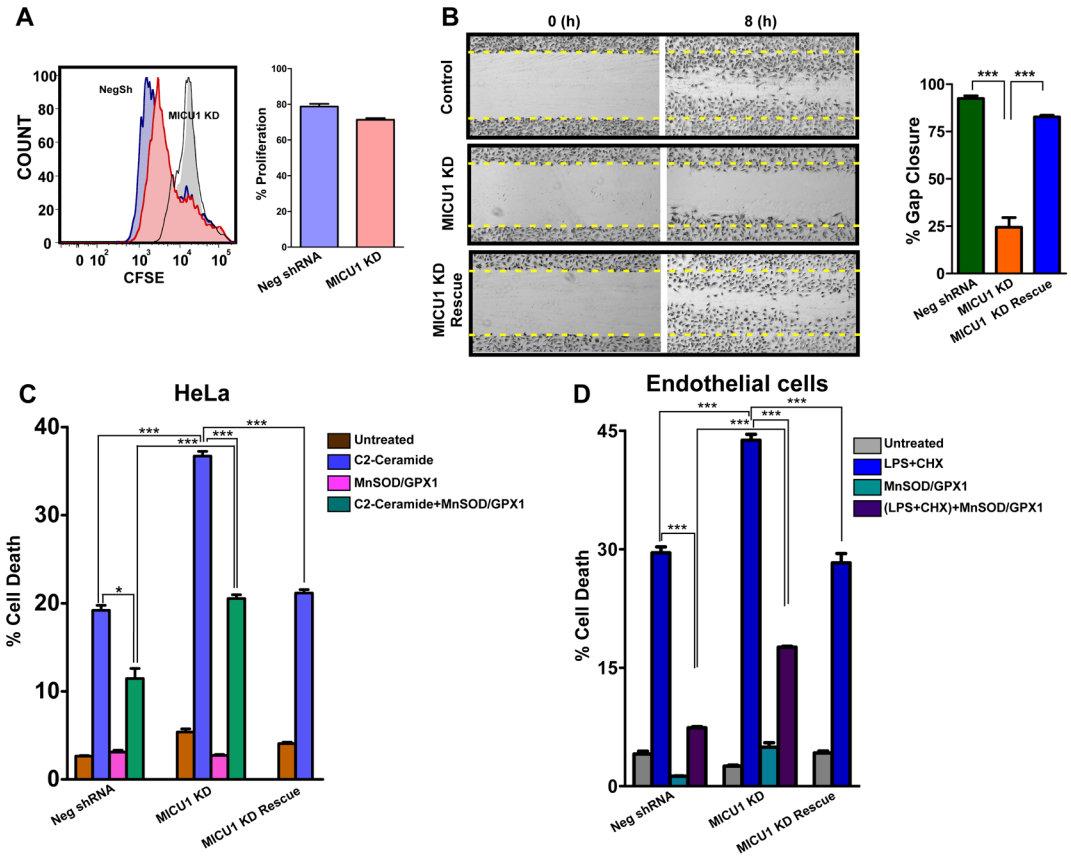

Figure 7. MICU1 Deficiency Impairs Cell Migration and Sensitizes Cells to Apoptotic Cell Death

(A) HeLa cells were labeled with CFSE and cell proliferation was determined by flow cytometry. Representative histograms (left) and quantification (right) of CFSE distribution after 72 hrs. Mean ± SEM; n=3.

(B) Representative images and quantification of cell migration in Neg shRNA, MICU1KD and MICU1 rescue ECs 8 hrs post scratch. Mean ± SEM; n=3.

(C) Quantification of cell death after 20 hrs of C2-Ceramide (40 μM) treatment. Neg shRNA and MICU1 KD cells treated with adenoviral manganese superoxide dismutase (MnSOD) and glutathione peroxidase 1 (GPX1) for 36 hrs before challenged with C2-Ceramide for 20 hrs; Mean ± SEM; *, ***: $P < 0.05$ and 0.001, respectively; n=3.

(D) Quantification of cell death in endothelial cells after 12 hrs of LPS and cycloheximide treatment. Neg shRNA and MICU1 KD endothelial cells treated with adenoviral MnSOD and GPX1 for 36 hrs before challenge with LPS and cycloheximide for 12 hrs; Mean ± SEM; ***: $P < 0.001$; n=3.